International Journal of Heat and Mass Transfer 53 (2010) 5651–5662

Contents lists available at ScienceDirect

International Journal of Heat and Mass Transfer

journal homepage: www.elsevier.com/locate/ijhmt

Significance of blood vessels in optimization of absorbed power and temperature distributions during hyperthermia

Huang-Wen Huang [a], Chihng-Tsung Liauh [b], Tzu-Ching Shih [c], Tzyy-Leng Horng [d], Win-Li Lin [e,*]

[a] Department of Innovative Information and Technology, Software Engineering Group, Langyang Campus, Tamkang University, I-lan, Taiwan
[b] Department of Mechanical Engineering, Kun-Shan University, Tainan, Taiwan
[c] Department of Biomedical Imaging and Radiological Science, China Medical University, Taichung, Taiwan
[d] Department of Applied Mathematics, Feng Chia University, Taichung, Taiwan
[e] Institute of Biomedical Engineering, College of Medicine and College of Engineering, National Taiwan University, No. 1, Section 1, Jen-Ai Road, Taipei, Taiwan

ARTICLE INFO

Article history:
Available online 16 September 2010

Keywords:
Thermally significant blood vessels
Hyperthermia
Temperature distribution
Absorbed power deposition
Optimization

ABSTRACT

This study investigated the significance of blood vessels in the absorbed power and temperature distributions when optimization was employed during hyperthermia. The treated tumor region was simulated using a three-dimensional (3D) tissue model embedded with a countercurrent blood vessel network (Huang et al., 1996). 3D temperature distributions are obtained by solving the conduction equation in the tissues and the convective energy equation with specified Nusselt number in the vessels. 3D absorbed power depositions are obtained by using optimization to reach a uniform temperature of 43 °C for the desired treated region. Results show that the absorbed power deposition for optimization with fine spatial resolution produces a uniform temperature distribution maintained at 43 °C in the desired treated tumor region except for some cold spots and/or small cold strips caused by thermally significant large vessels. The amount of total absorbed power suggests that a region with thermally significant vasculature requires much more power deposited than one without vasculature. In addition, optimization with coarse spatial resolution results in a highly inhomogeneous temperature distribution in the treated region due to the strong cooling effect of blood vessels. Therefore, prior to hyperthermia treatments, thermally significant blood vessels should be identified and handled carefully to effectively reduce their strong cooling effect, particularly those vessels flowing into the treated region.

© 2010 Elsevier Ltd. All rights reserved.

1. Introduction

Hyperthermia cancer treatment requires precise thermal absorbed power deposition to raise tumor tissue temperature up to the therapeutic range with a sufficient amount of time duration and to prevent overheating the normal tissues. Many researchers [1–4] have investigated noninvasive heating modality for exploring power deposition with fine spatial resolution and/or optimization within the tumor region. Hyperthermia applicator technology is currently one of the most important issues that can improve temperature homogeneity in the treated region as well as reach optimal applied power deposition.

The Pennes' bio-heat transfer equation (BHTE) [5] has been a standard model for predicting temperature distributions in living tissues. The equation was established through conducting a sequence of experimental temperature measurements of tissue and arterial blood temperatures in the resting human forearm. The equation includes a special term that describes the heat exchange between blood perfusion and solid tissues. The blood temperature is assumed to be constant arterial blood temperature. The main limitation of this equation is its inability to describe the impact of thermally significant vessels. Some researchers [6–10] have also developed alternative equations having the same goal of attempting to formulate a single, general field equation that can predict the overall characteristics of temperature distributions in tissues. Those approximate field equations, which are intended to predict the average thermal behavior of the tissue, do not have the ability to accurately model the effects of isolated, large vessels. Thus, such blood vessels must be modeled using separate equations. The effects of such vessels have been studied by Chato [11] and Huang et al. [12], and Huang [13] developed analytical models for single vessels. Other investigators [14–23] have done numerical and experimental hyperthermia studies for single vessels and/or counter current vessel pairs embedded in either a purely conductive media (with either a normal thermal conductivity, or an enhanced, effective thermal conductivity) or in media modeled by the Pennes' BHTE. One example, published by Rawnsley et al. [21], illustrated the experimental temperature data measured in the thighs of

* Corresponding author. Tel.: +886 2 2312 3456x81445; fax: +886 2 2394 0049.
E-mail address: winli@ntu.edu.tw (W.-L. Lin).

0017-9310/$ - see front matter © 2010 Elsevier Ltd. All rights reserved.
doi:10.1016/j.ijheatmasstransfer.2010.08.017

Nomenclature

c	specific heat capacity, J kg^{-1} C^{-1}
C	cost function
D	diameter of blood vessel, mm
h_{coef}	updated power coefficient
H	length of control volume in z direction, cm
k	thermal conductivity, W m^{-1} C^{-1}
L	length of control volume in x direction, cm
m	mass flow rate, kg s^{-1}
Nu	Nusselt number of blood vessels
P	absorbed power deposition, W m^{-3}
q	absorbed thermal power, W m^{-3}
R	radius of blood vessel, mm
T	temperature, °C
w	perfusion rate, kg m^{-3} s^{-1}
W	length of control volume in y direction, cm
x	coordinate in the x direction
y	coordinate in the y direction
z	coordinate in the z direction
ΔCn	cost function increment at nth iteration
ΔT	temperature difference, °C

Greek symbols

γ	ratio of diameters of successive levels of branching arteries
π	mathematical constant
ρ	density, kg m^{-3}

Subscripts

adj	adjacent tissue temperature
b	blood
bv	blood vessel
i	index of node number; index of level number of blood vessels
n	iteration
s	absorbed source power
vr	venous returning terminal vessels
w	vessel wall

anesthetized greyhound dogs under hyperthermic conditions heated by scanned focused ultrasound. When small numbers (3) and (4) of blood vessel pairs were included in Pennes' bio-heat transfer thermal model, the model showed significant improvement in its ability to predict experimental temperatures. Leeuwen et al. [22] also stressed that efforts to obtain information on the positions of the large vessels in an individual hyperthermia patient could be rewarded with a more accurate prediction of the temperature distribution. Finally, a few studies [22,24–26] have modeled the effect of collections of a large number of parallel vessels or of networks of vessels on the resulting temperature distributions. However, those studies did not consider optimization in hyperthermia treatments.

This study investigated the impact of thermally significant blood vessels on hyperthermia treatment using a thermal conduction matrix model embedded with a network of blood flow vessels (fully conjugated blood vessel network model (FCBVNM), Huang et al. [24]). Optimization was used to determine the power deposition to achieve an ideal 3D therapeutic temperature distribution with a uniform temperature of 43 °C for the desired treated region. Optimized absorbed power deposition with fine/coarse spatial resolution was considered to study the effects of thermally significant blood vessels on the resulting temperature distributions and the limitation of heating ability for power systems.

2. Methods

2.1. Vessel network geometry and fully conjugated blood vessel network model (FCBVNM)

FCBVNM is a model formulation which describes the solid tissue matrix having thermally significant vessel generations (seven levels). The effects of all vessels smaller than the terminal (level seven) vessels are not explicitly modeled in FCBVNM. Thus, those smaller vessels (connected to the terminal arteries and the terminal veins in the network) are implicitly assumed to be thermally insignificant in the FCBVNM.

The tissue geometry used in this study consists of a regular, branching vessel network as partially shown (only the arterial vessels are shown) in Fig. 1 that is embedded in a control volume, which is an (approximate) cube of dimensions $L = 8.2$ cm and $W = H = 8$ cm in the x, y, and z directions, respectively. All vessels are straight-line segments parallel to one of the three Cartesian axes. There are up to seven levels of arteries, beginning with the main artery (level one) which lies along the central, lengthwise (x) axis of the cube. Table 1 of Huang et al. [24] lists the basic vessel network properties used in this study. The diameters of the arteries decrease by a constant ratio γ between successive levels of branching vessels (the ratio of diameters of successive vessel generations), i.e.

$$\gamma = \frac{D_{i+1}}{D_i} \tag{1}$$

where D_i and D_{i+1} are the diameters of two successive levels of branching arteries. When two successive levels of numbered vessels do not branch but only change direction (i.e., levels six and seven in this model), the vessel diameter does not change. In this study, we used $\gamma = 0.9$ in the presented results.

The desired treated tumor region is a cube described in Fig. 2(a) with 20 mm in x, y and z dimensions. The locations and paths of arterial vessels inside the treated region are described in Fig. 2(b) and (c). The geometric arrangement of the countercurrent veins is essentially identical to that of the arteries, with all of the veins offset from the arteries by one finite difference node in x, y, and z dimensions as appropriate to avoid intersections of vessels.

2.2. Mathematical equations for the thermal model

The governing equation in tissues is described below,

$$\nabla \cdot (k\nabla T(x,y,z)) - \dot{w}_b c_b (T(x,y,z) - T_a) + q_s = 0 \tag{2}$$

where k, c_b, w_b, and q_s are the thermal conductivity of soft tissue, specific heat of blood, blood perfusion rate and absorbed thermal power density, respectively. T_a is the arterial blood temperature and may be replaced by $T_b(x, y, z)$ only if blood temperature is from terminating arterial vessels. The metabolism effect is neglected in Eq. (2) due to its limited effect on temperature distribution during hyperthermia.

The convective energy equation is solved for the FCBVNM model,

$$m_{b,i} c_b \nabla T_b(x,y,z) = Nu \cdot k_b \pi (T_w(x,y,z) - T_b(x,y,z)) + q_s \pi R_{bv,i}^2 \tag{3}$$

where $m_{b,i}$ is the blood mass flow rate at level i vessel segment. Nu, k_b, $R_{bv,i}$ and T_w are Nusselt number, thermal conductivity in blood, radius of blood vessel at level i and blood vessel wall temperature.

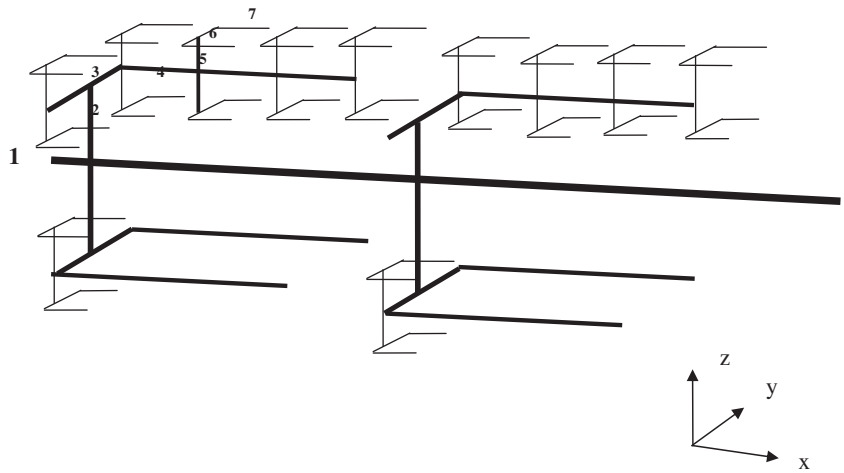

Fig. 1. Schematic diagram to show portion of the arterial vessel network used in this study. All seven vessel levels (levels 1–7) for the arterial network are shown, and the venous network, which is not shown, is parallel to the arterial network, with a grid size in the *x*, *y*, and *z* dimensions away from the arterial network.

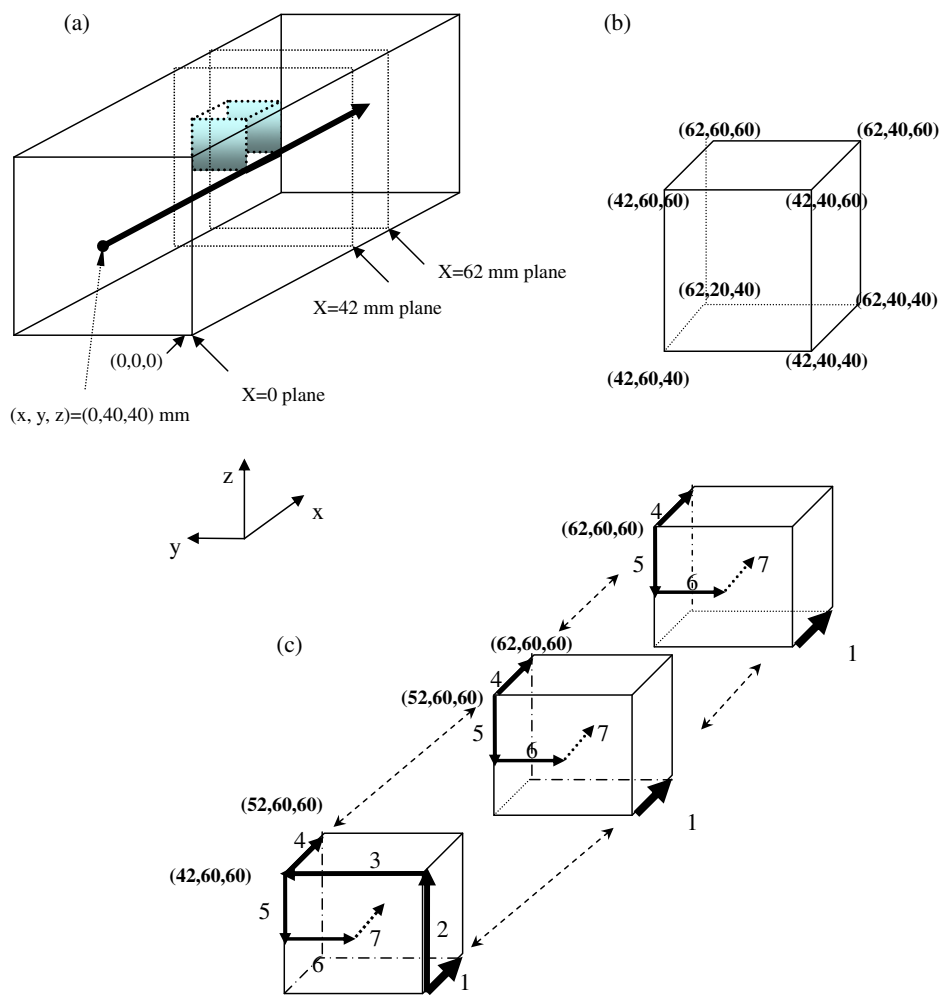

Fig. 2. (a) A transparent view of parallelepiped showing the desired heated tumor region, which is a cube of 20 mm in each dimension. The level 1 blood vessel (the largest) runs through the desired heated cube's edge from (42, 40, 40) to (62, 40, 40). The inlet temperature of the level 1 vessel starting at (0, 40, 40) is set at 37 °C. (b) shows the coordinates of 8 corners of the desired treated cube (unit: mm). (c) is a dissected transparent view showing all associated arterial blood vessel paths (or segments) in the cubic volume, and venous vessels do not appear in the figure. There are two branches of levels 5–6–7 blood vessels and one of levels 5–6 on the back boundary as the dissected view indicates.

A total of 682 vessels in the model need to be calculated using Eq. (3). That is, *i* is from 1 to 682 for Eq. (3). Constant blood bleeding or collection along the vessels is considered for 128 arterial and 128 venous terminal ends of level 7 vessels.

To simulate the relationship between blood flow and perfusion in tissues, the following equation is used:

$$m_{b,i}c_b\nabla T_b(x,y,z) = Nu\cdot k_b\pi(T_w(x,y,z) - T_b(x,y,z)) + q_s\pi R_{bv,i}^2 - \frac{dm_{b,i}}{dx}\cdot c_bT_b(x,y,z) \quad (4)$$

In Eq. (4), $dm_{b,i}/dx$ is the constant blood bleeding or collecting mass rate at any cross-section along terminal ends, as the vessels linearly perfuse blood into local tissue environments (i.e. subvolumes) or collect blood from local tissue environments. That is, for the smallest terminal arterial vessels (level 7), a decreasing blood flow rate is present.

For venous return thermal model, assuming all of the blood which has perfused a terminal subvolume is collected at any cross-section by the terminal vein associated with that subvolume, the following equation is used to calculate the blood temperature in terminal veins

$$T_{vr} = \frac{1}{4}\sum_{i=1}^{4} T_{i,adj} \quad (5)$$

where $T_{i,adj}$ is the tissue temperatures adjacent to venous vessel. As a terminal vessel runs in any x, y or z straight direction, there are four neighboring tissue nodes considered in terms of computational scheme (i.e. finite difference method). For graphically illustrating the models and assumptions above, Fig. 3 shows models depicting Eqs. (3)–(5).

The conservation of energy equation is applied for those locations where branching vessels occur. Calculation of the blood temperature in vessels with a steady uniform velocity profile for blood flow has been used widely and accepted in many studies. Recently, Horng et al. [27] reconfirmed the usage of steady uniform velocity profile approach. Conduction occurs in all three directions in the tissue matrix, and the outer control volume surface is held at a constant reference temperature (i.e. identical to the inlet artery temperature).

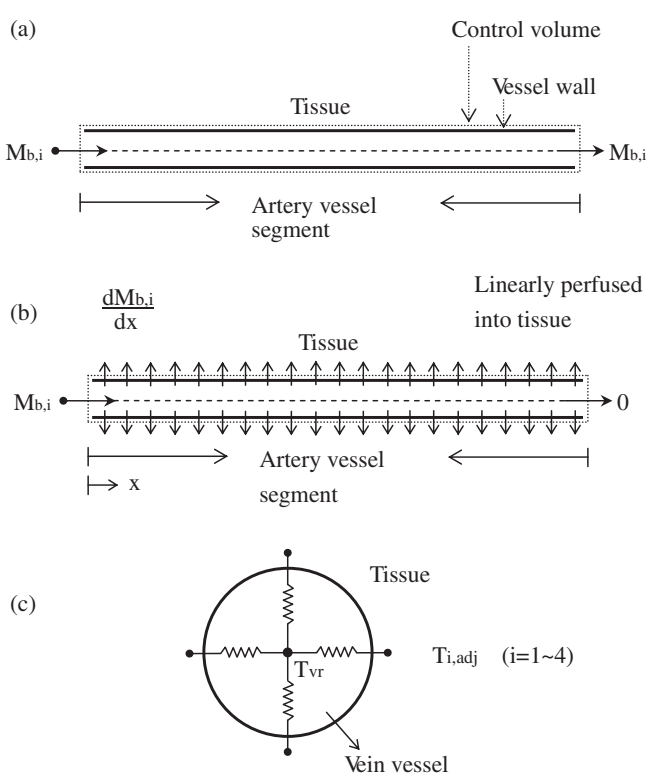

Fig. 3. (a) The model used for non-terminal artery blood vessels in which the convective energy equation (3) is solved for the FCBVNM model. $M_{b,i}$ is the blood flow rate entering vessel i and leaving with identical mass flow rate $M_{b,i}$. (b) The model used for the artery terminal vessels (level 7) as explained in Eq. (4). $M_{b,i}$ is the blood flow rate entering vessel i with linearly perfused mass flow rate into tissue of $dM_{b,i}/dx$. (c) The model of calculating returning vein blood temperature, as explained in Eq. (5).

2.3. Optimization with fine spatial power deposition: based on local temperature response in the treated region

Fig. 4 is the flow chart to describe continuously adjusting absorbed power deposition in the desired treated tumor region in order to reach ideal temperature (uniform temperature throughout the treated tumor region with a temperature of 43 °C). The evaluation criterion of absorbed power deposition is shown in Eq. (6), which states that root mean square of difference of ideal temperature (43 °C) and calculated temperature of all heated target nodes divided by (43 − 37) °C reaches less than the criterion value (set to be 10% of the temperature difference of (43 − 37) °C). If the criterion is achieved, we obtain the optimization of absorbed power deposition such that the heating temperature distribution is close to the ideal temperature distribution. Otherwise, the absorbed power deposition will be adjusted according to the local temperature. The readjusted power deposition (P_{n+1}) is described in Eq. (7)

$$\text{Evaluation criterion}: \quad \frac{\sqrt{\frac{\sum_{\text{all target nodes}}(\Delta T(x,y,z))^2}{\text{Total number of target nodes}}}}{(43-37)\,^\circ C} \leqslant 0.1 \quad (6)$$

$$P_{n+1}(x,y,z) = P_n(x,y,z) + \Delta P(x,y,z) \quad (7)$$

with $\Delta P(x,y,z) = Coef\cdot\Delta T(x,y,z)$, $Coef$ is 10,000, n is the iteration number and $\Delta\ T(x,y,z)$ is the difference of ideal temperature (43 °C) and calculated temperature.

2.4. Optimization with lumped power deposition: uniform absorbed power deposition in the treated tumor region

To investigate the spatial resolution of absorbed power deposition on the temperature distribution, a uniform power deposition in the entire desired treated tumor region is applied. Two important parameters need to be introduced for this optimization. One is cost function and the other is the power coefficient. Cost function is set to be $C_n = \sqrt{\sum_{\text{all target nodes}}(T(x,y,z) - 43\,^\circ C)^2}$ at nth iteration, and the absorbed power is $P_{n+1} = P_n + h_{coef}\cdot\Delta C_n$, with $\Delta C_{n+1} = C_{n+1} - C_n$ and the coefficient h_{coef}. h_{coef} is the updated power coefficient, with a constant value of 3050. It is chosen based on a smoothly converging (i.e., no oscillating) search and with less computational time required during optimization. The optimization process will be terminated when ΔC_n is smaller than 10^{-4}. With optimization of uniform power deposition, it allows the attention to be focused on the effect of the vasculature on the temperature distribution.

2.5. Numerical methods

The numerical scheme used to calculate the temperatures was a black and red finite difference SOR method [28] with upwind differencing used for the vessels. The numerical details are described by Chen [29] and Hunag [13]. Special algorithms are used to account for the vessel corners where arteries and veins change direction, and where two or more arteries divide, or two or more veins join. The thermal resistances around the circular vessels were calculated using the logarithmic resistance approach as described by Chen and Roemer [30]. The property values used in treated tumorous and non-treated normal tissues were $k = 0.5\ \text{W m}^{-1}\,^\circ\text{C}^{-1}$,

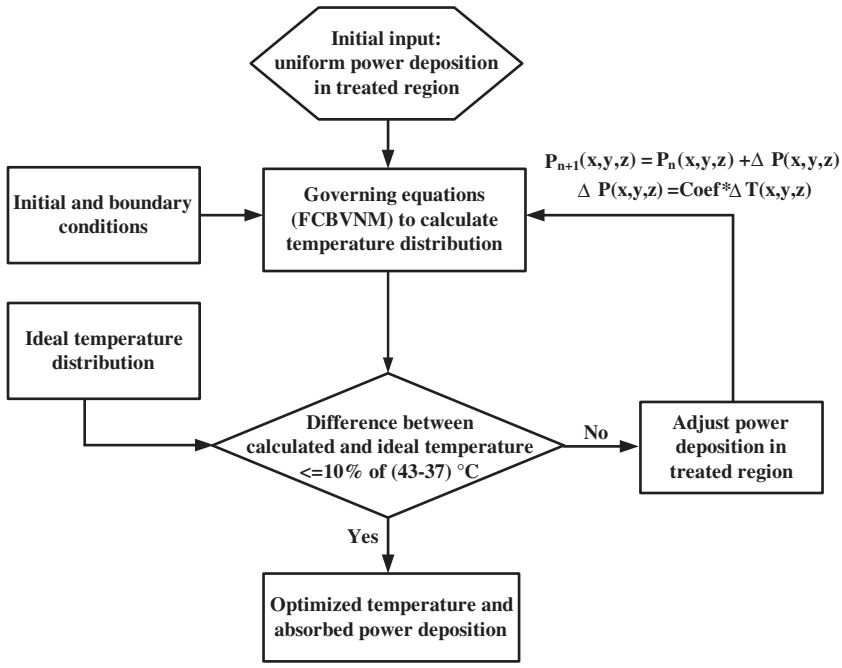

Fig. 4. The flow chart of optimization used in this study. The absorbed power deposition in the desired treated cube (20 mm in each dimension) is adjusted locally in order to achieve an ideal therapeutic temperature of 43 °C uniformly for the entire cube.

$c = c_b = 4000\ J\ kg^{-1}\ °C^{-1}$ and $\rho = 1000\ kg\ m^{-3}$. The vessel heat transfer coefficient was calculated using a constant Nusselt number of four for all vessel levels. In all cases, a finite difference nodal spacing of 2 mm was used. Test results with a nodal spacing of 1 mm for test cases using either the arterial vessel network (when no veins were present) or the countercurrent vessel network showed no significant differences with the results of the comparable 2-mm nodal spacing models. This 2-mm spacing gives an inter-vessel centerline to centerline diagonal spacing of 2.8 mm for the countercurrent vessels due to the 2-mm offsets in *x*, *y*, and *z*. The boundary temperature was set to 37 °C at the outer control volume surfaces. Inlet temperatures of (level 1) vessels to the control volume were also set to 37 °C.

3. Results

3.1. Optimization with fine spatial power deposition: based on local temperature response

To investigate the significance of blood vessels in the temperature distribution for optimal hyperthermia treatment, an optimization scheme as shown in the method section was employed to determine the absorbed power deposition, which included the heating of blood vessels to achieve an optimal treatment. Fig. 5(a)–(e) is the optimal temperature distributions on the planes 4 mm away from the front boundary, the front boundary, the middle, the back boundary, and 4 mm away from the back boundary of the treated region, respectively, and Fig. 5(f)–(h) is the absorbed power depositions on the planes of the front boundary, the middle, and the back boundary of the treated region, respectively, for a blood perfusion of 0.5 kg m^{-3} s^{-1} and a blood flow velocity of 320 mm s^{-1} in the level 1 vessel. Fig. 5(a) shows that the temperature is approximately 40.0 °C near the treated region and displays a cold spot at the center which is due to level 1 artery blood vessel running perpendicular inwards to the plane. At its southeastern diagonal direction about 2.8 mm away from the level 1 artery, a level 1 vein blood vessel is running in an opposite direction outwards to the plane. The vein appears to be collecting some thermal energy by convection through treated region. Fig. 5(b) shows that the temperature on the boundary of the treated region is close to ideal temperature (43 °C), and there are steep thermal gradients near the level 2 artery running upwards from the center point. As seen in Fig. 5(f), large amounts of thermal power were deposited on levels 2, 3 and 5 arteries. The maximum thermal power deposition is approximately 3.7×10^6 W m^{-3}. Fig. 5(c) shows that the temperature in the treated region is close to ideal temperature, while high temperature appears outside of the treated region due to a level 6 artery carrying convective thermal energy leftwards. It illustrates that thermally significant blood vessels within the treated region have effectively been heated and carried the convective thermal energy out of the region. Fig. 5(c) also shows maximum temperature located on (or near) left-side artery branch node of levels 5 and 6 arteries in the treated region. Fig. 5(g) shows large thermal power is deposited on the corner of treated region, which is an area with dense blood vessels (levels 3, 4 and 5 arteries and veins). Fig. 5(d), the temperature distribution at the back boundary of the treated region, shows that a cold spot is found near the northwestern corner of heated region. The spot is 1.7 °C below the ideal temperature, and it is caused by the level 4 vein flowing into the heated region. As expected, Fig. 5(h) shows large amount of thermal power deposited on the same corner as shown in Fig. 5(g) to compensate the heat loss caused by vessels. Dense blood vessels act as energy sinks, and large amount of thermal power deposition is required in that area in order to maintain the local temperature at the desired level. Fig. 5(e), temperature on the plane 4 mm away from the back boundary of the heated region, shows some hot spots, and these spots are approximately 42 °C. One spot, located in the northeastern direction more than 4 mm away from the heated region, has a temperature of about 38.3 °C. Those hot spots are caused by arteries carrying hot blood flow.

3.2. Effect of blood perfusion and blood flow rates on the optimization

As blood perfusion increases, the flow rates in vessels get higher due to the conservation of blood mass, and the higher flow rate will produce a stronger thermal impact on the treated region. Fig. 6

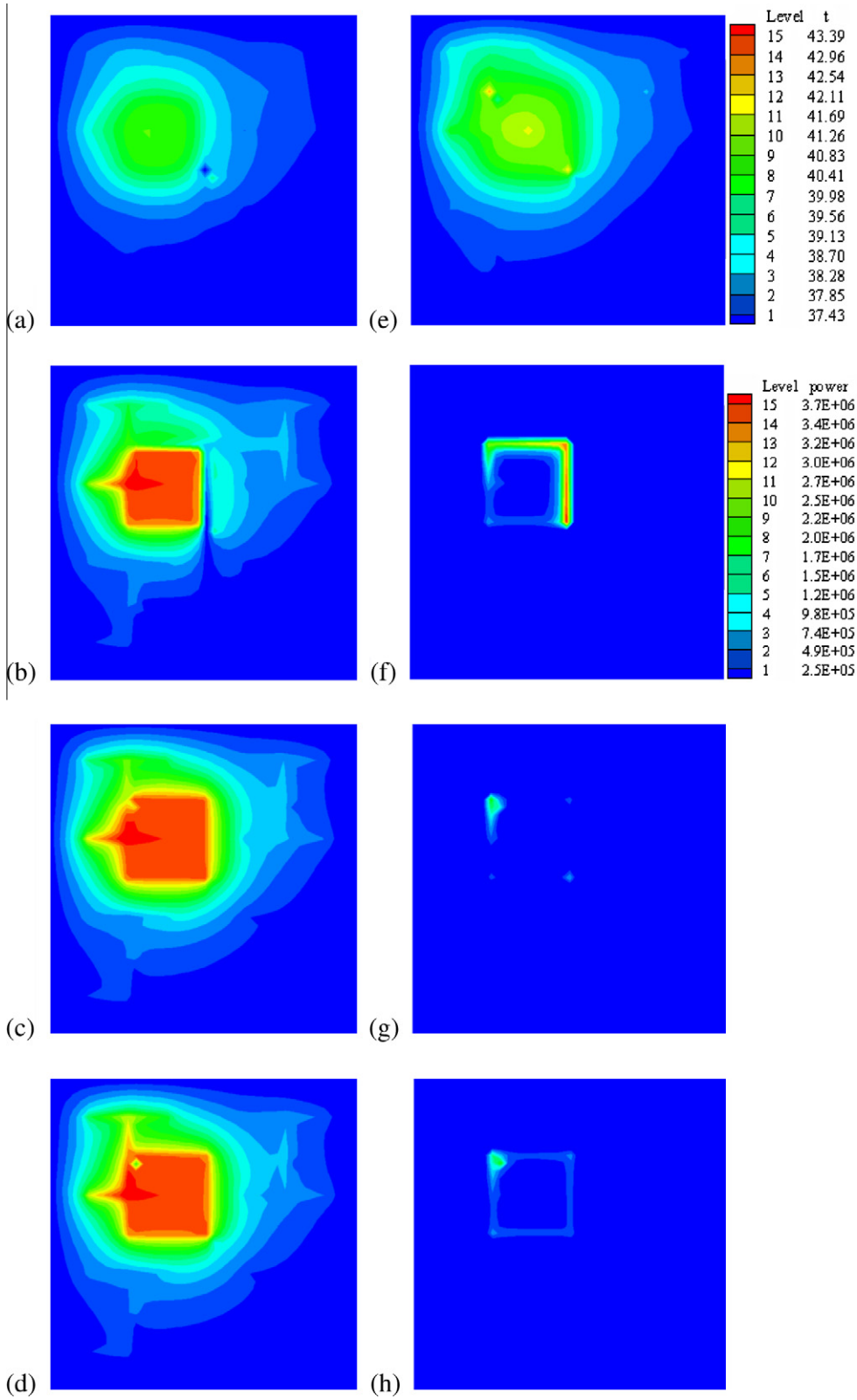

Fig. 5. Temperatures and absorbed power depositions for a blood perfusion rate of 0.5 kg m^{-3} s^{-1} after optimization with fine spatial power deposition. The ideal temperature is set to be 43 °C, and the blood flow velocity is about 320 mm s^{-1} in level 1 vessel. (a)–(e) are the temperature distributions at x = 38 mm (4 mm away from the front boundary), x = 42 mm (the front boundary), x = 52 mm (the middle of the treated region), x = 62 mm (the back boundary) and x = 66 mm (4 mm away from the back boundary) planes, respectively. (f)–(h) are the absorbed power depositions at x = 42 mm, 52 mm and 62 mm planes, respectively, after optimization (units in figure, temperature: °C and power density: W m^{-3}).

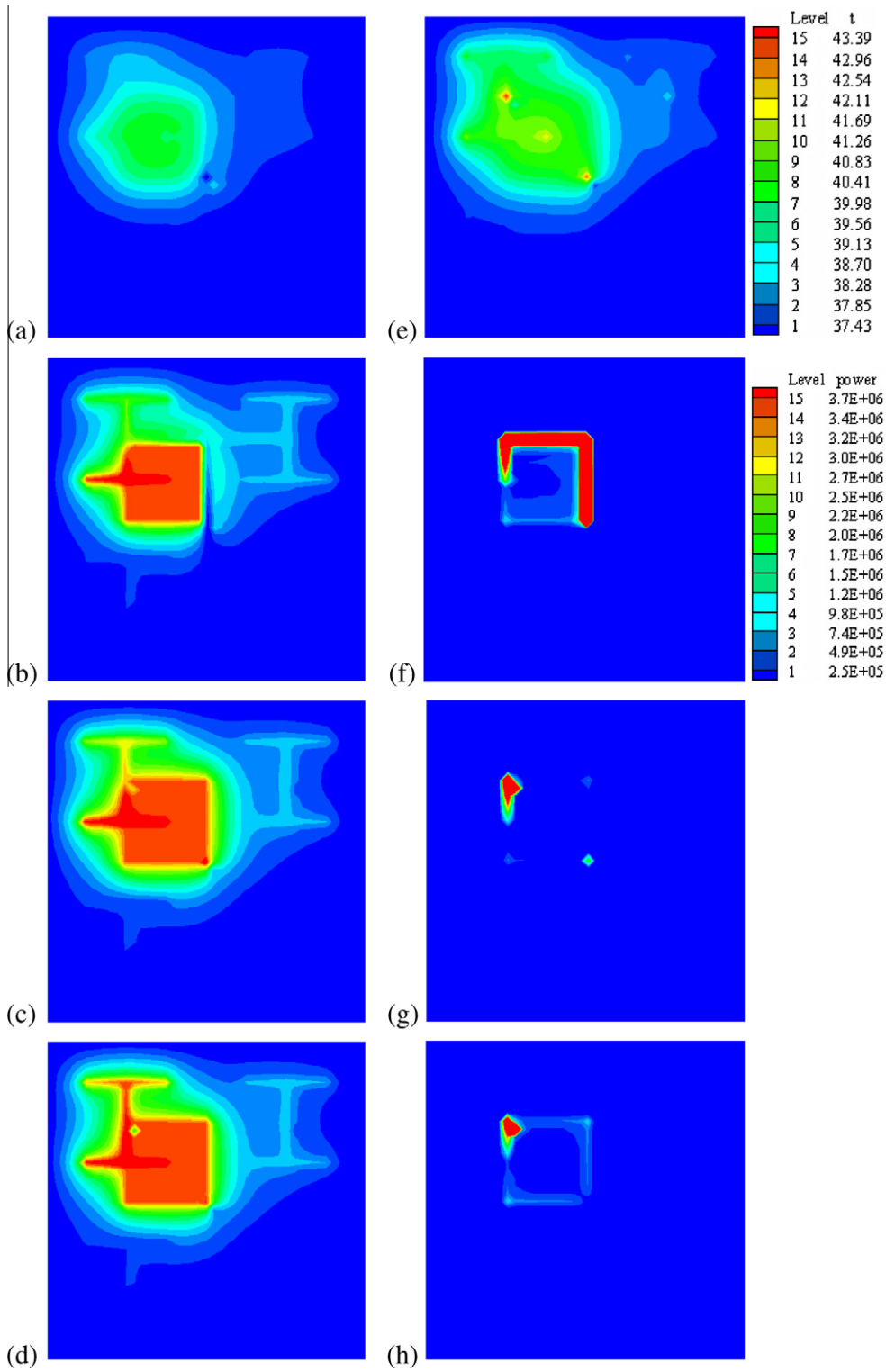

Fig. 6. Temperatures and absorbed power depositions for a blood perfusion rate of 2.0 kg m^{-3} s^{-1} after optimization with fine spatial power deposition. The ideal temperature is set to be 43 °C, and the blood flow velocity is about 1280 mm s^{-1} in level 1 vessel. (a)–(e) are the temperature distributions at x = 38 mm (4 mm away from the front boundary), x = 42 mm (the front boundary), x = 52 mm (middle of the treated region), x = 62 mm (the back boundary) and x = 66 mm (4 mm away from the back boundary) planes respectively after optimization. (f)–(h) are the absorbed power depositions at x = 42 mm, 52 mm and 62 mm planes, respectively, after optimization (units in figure, temperature: °C and power density: W m^{-3}).

shows temperature and power depositions for a blood perfusion of 2.0 kg m^{-3} s^{-1} and a blood flow velocity about 1280 mm s^{-1} in level 1 blood vessel. Fig. 7 shows temperature and power depositions for a blood perfusion of 0.123 kg m^{-3} s^{-1} and a blood flow velocity of about 80 mm s^{-1} in level 1 blood vessel, which in size and blood flow velocity of vessel is identical to dog data from Chen and

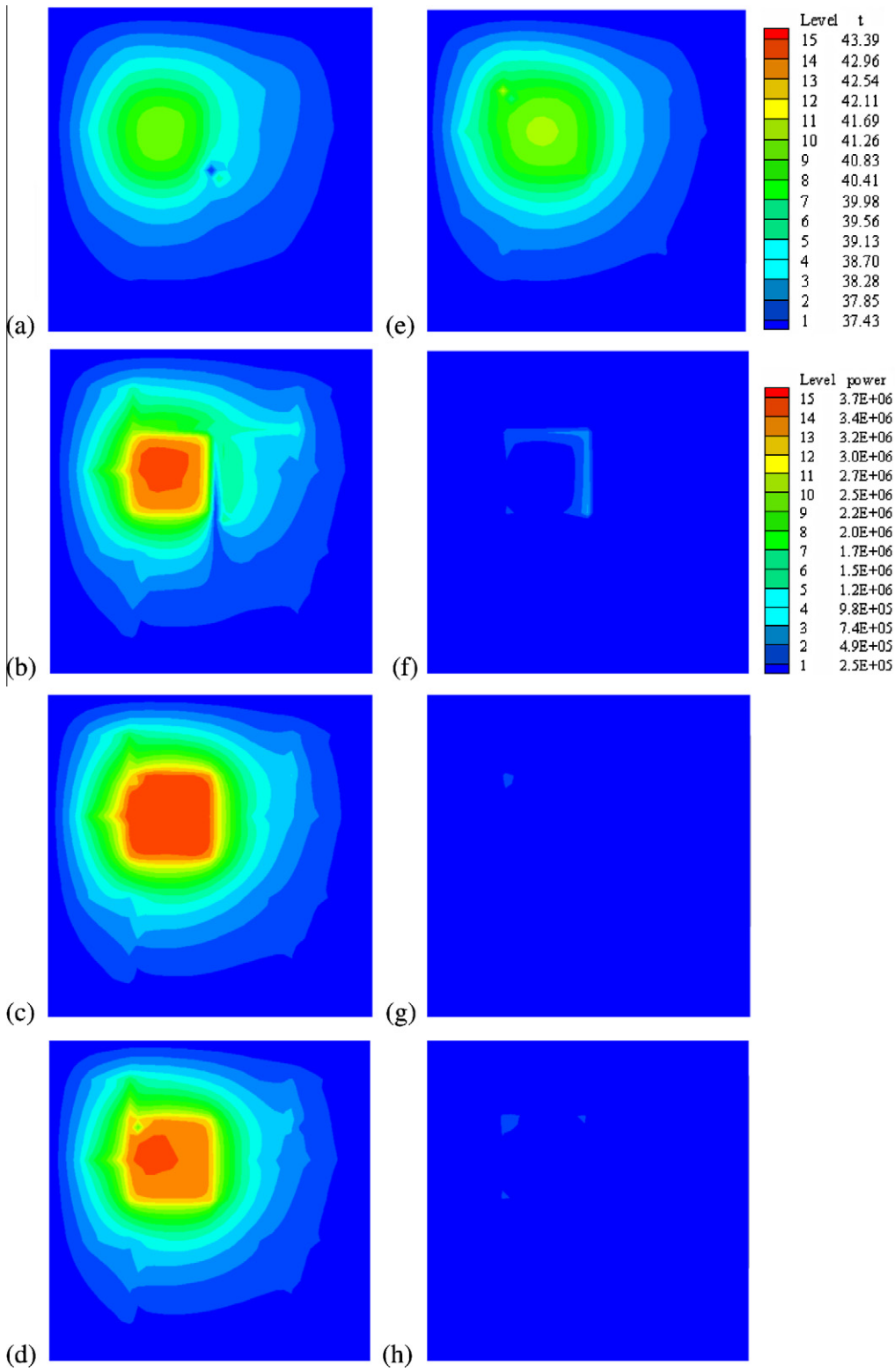

Fig. 7. Temperatures and absorbed power depositions for a blood perfusion rate of 0.123 kg m^{-3} s^{-1} after optimization with fine spatial power deposition. The ideal temperature is set to be 43 °C, and the blood flow velocity is about 80 mm s^{-1} in level 1 vessel. (a)–(e) are the temperature distributions at x = 38 mm (4 mm away from the front boundary), x = 42 mm (the front boundary), x = 52 mm (middle of the treated region), x = 62 mm (the back boundary) and x = 66 mm (4 mm away from the back boundary) planes, respectively, after optimization. (f)–(h) are the absorbed power depositions at x = 42 mm, 52 mm and 62 mm planes, respectively, after optimization (units in figure, temperature: °C and power density: W m^{-3}).

Holmes [6]. The optimized power deposition pattern is similar to but with a higher or lower value than that shown in Fig. 5, and the temperature distribution displays that uniform temperature close to the ideal value can be obtained in the treated region except for some cold spots which are produced by the arteries same as the case of 0.5 kg m^{-3} s^{-1}.

3.3. Optimization without thermally significant blood vessels in the tissues

Pennes' bio-heat transfer equation is used to investigate temperature and absorbed power deposition in the treated region for the condition without thermally significant blood vessels. A uniform blood perfusion rate of 0.5 kg m^{-3} s^{-1} in the entire tissue was studied using the optimization. Fig. 8(f)–(h) shows the optimized power deposition on the front boundary, the middle and the back boundary planes, respectively. Most of the power is deposited on the corners and edges of the treated region to compensate for thermal energy loss through conduction due to the

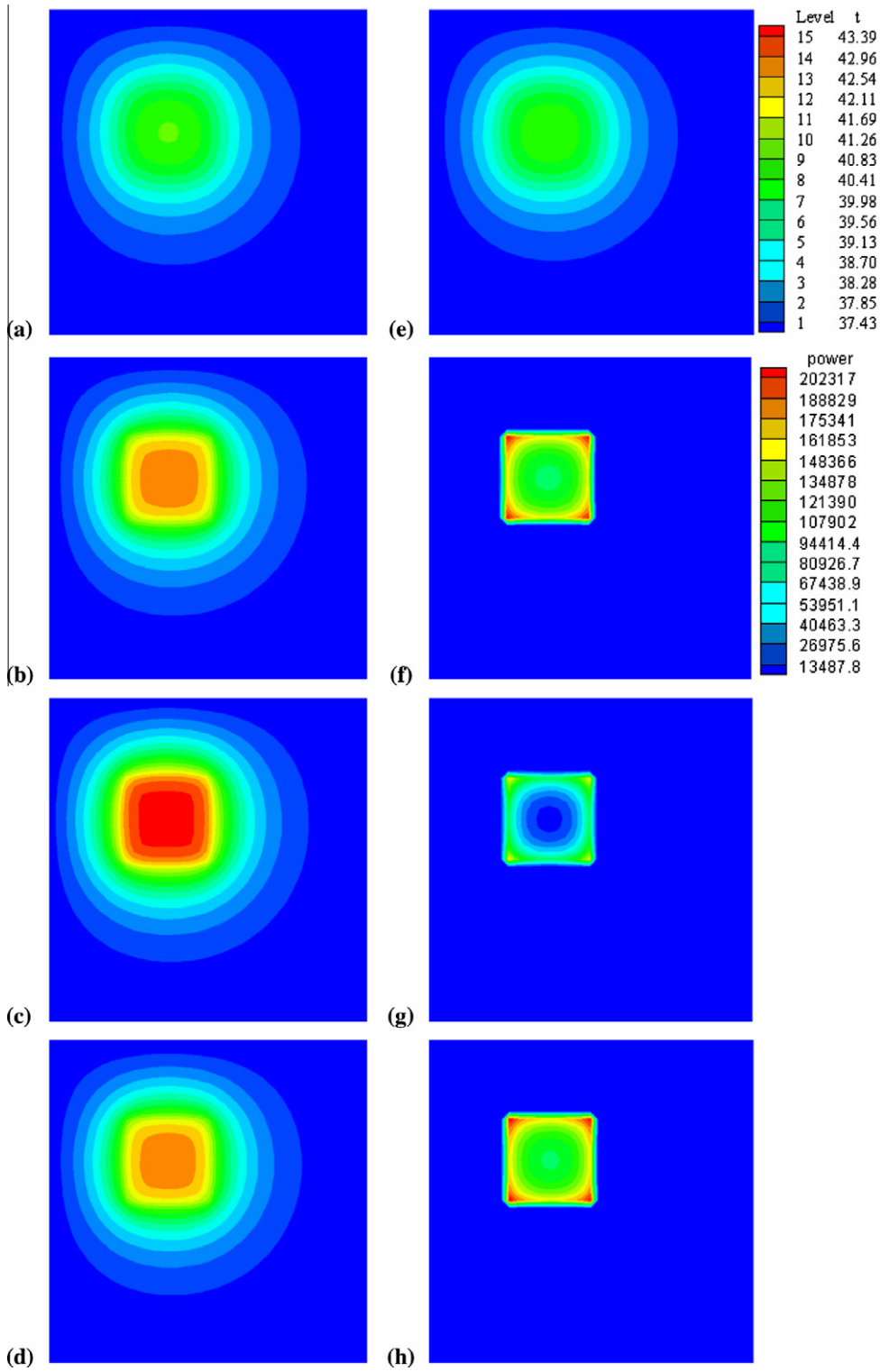

Fig. 8. Temperatures and absorbed power depositions for a blood perfusion rate of 0.5 kg m^{-3} s^{-1} with no vasculature present and after optimization with fine spatial power deposition. The ideal temperature is set to be 43 °C. (a)–(e) are the temperature distributions at x = 38 mm (4 mm away from the front boundary), x = 42 mm (the front boundary), x = 52 mm (middle of the treated region), x = 62 mm (the back boundary) and x = 66 mm (4 mm away from the back boundary) planes respectively after optimization. (f)–(h) are the absorbed power depositions at x = 42 mm, 52 mm and 62 mm planes, respectively, after optimization (units in figure, temperature: °C and power density: W m^{-3}).

strong conductive effects near corners and edges. The deposited power pattern of Fig. 8(h) is identical to that shown in Fig. 8(f) and (g) (the middle plane of the treated region) displays that there is less power deposited on corners and center area as compared to Fig. 8(f) (the front boundary plane). It indicates that the thermal diffusion rate is much smaller in the middle region. Fig. 8(b)–(d)

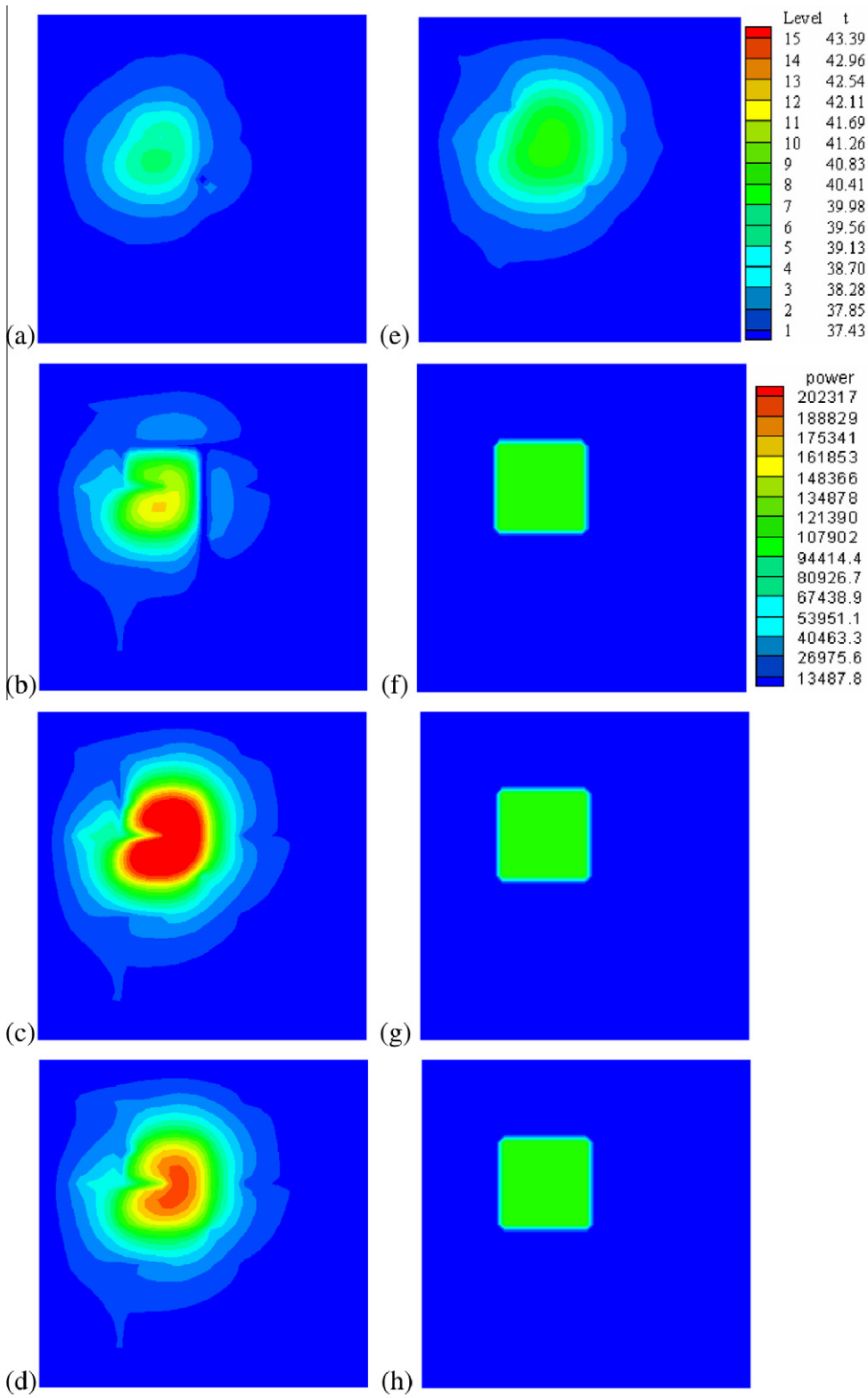

Fig. 9. Temperatures and absorbed power depositions for a blood perfusion rate of 0.5 kg m^{-3} s^{-1} after optimization with lumped power deposition. The ideal temperature is set to be 43 °C, and the blood flow velocity is about 320 mm s^{-1} in level 1 vessel. (a)–(e) are the temperature distributions at x = 38 mm (4 mm away from the front boundary), x = 42 mm (the front boundary), x = 52 mm (the middle of the treated region), x = 62 mm (the back boundary) and x = 66 mm (4 mm away from the back boundary) planes, respectively. (f)–(h) are the absorbed power depositions at x = 42 mm, 52 mm and 62 mm planes, respectively after optimization (units in figure, temperature: °C and power density: W m^{-3}).

shows that a very uniform therapeutic temperature distribution in the treated region can be achieved as there are no thermally significant blood vessels present.

3.4. Optimization with lumped power deposition in the treated region

To investigate the effect of lumped power deposition on the resulting temperature distribution, a uniform power deposition for the entire treated region was used. This represents the limitation of the heating system to tune its power spatially fine enough to meet the treatment requirement. Fig. 9(a)–(e) is the optimized temperature distributions on the planes of 4 mm away from the front boundary, the front boundary, the middle, the back boundary, and 4 mm away from the back boundary of the treated region, respectively, and Fig. 9(f)–(h) are absorbed power depositions on the planes of the front boundary, the middle and the back boundary, respectively, for a blood perfusion of 0.5 kg m^{-3} s^{-1} and a blood flow velocity of 320 mm s^{-1} in the level 1 vessel. The initial guess of the uniform power deposition in the treated region was 10^5 W m^{-3}, and the optimized absorbed power deposition was obtained as the difference (ΔC_n) between two successive cost function values was smaller than 10^{-4}. With this optimization of lumped power deposition, the temperatures shown in Fig. 9(b)–(d) indicate that the temperatures in the treated region are highly inhomogeneous, with a temperature about 3 °C below the desired therapeutic temperature in the places near the boundary planes. These temperature distributions display that blood flow of vessels results in a significantly lower temperature strips along the vessels in the treated region, particularly a large vessel located at the boundary of the treated region.

3.5. Comparison of total absorbed power in the treated region

Fig. 10 shows the total absorbed power in the treated region for different conditions of optimization. It illustrates that the power deposited for optimization with blood vessel (BV) present is much higher than that without blood vessels. The total power for optimization based on local temperature response to tune its power deposition to compensate the convective effect of blood vessels was greater than that for optimization with lumped power deposition. For a blood perfusion rate of 2.0 kg m^{-3} s^{-1} in the tissue, the total absorbed power was about 3.4 times of that for the case of 0.5 kg m^{-3} s^{-1}.

4. Discussion

With the purpose of investigating the optimized temperature distribution for hyperthermia treatment with thermally significant blood vessels in the treated region, we employed a vascular model with blood vessels embedded in the tissues and using optimization to tune power deposition to meet the treatment needs. In clinical practice, the location and geometry of vessels need to be obtained first either by magnetic resonance imaging (MRI) or ultrasound, and then optimization can be applied. Obtaining vessel information is a complicated and time-consuming task. Although the present study employed a simple vessel network model, it helped us develop the basic approach and illustrate the effect of blood vessels, which PBHTE could not describe.

Two optimization schemes were used in this study to represent the optimization for two extreme heating systems used in hyperthermia treatment: one with fine spatial power deposition, able to tune its local power according to each local temperature response, and the other one with lumped uniform power deposited in the entire treated region and able to be tuned its power level according to the cost function based on the entire temperature response. The former scheme was able to deposit enough power to heat the blood vessels and their adjacent areas to effectively limit the blood vessel cooling effect, while the latter one was not able to deliver enough power to cover the effect of blood vessels and resulting large cold strips along the vessels. This shows interesting heating situations in hyperthermia treatment: (1) blood vessels can carry convective energy and circulate to produce cold spots/strips in the desired treated region and hot spots/strips in the normal tissues and (2) a heating system with high resolution power deposition ability is required to effectively reduce the cooling effects of blood vessels during hyperthermia.

Existing thermally significant blood vessels in the treated region can generate cold strips or spots during optimization of hyperthermia treatment. It is of vital importance to identify all thermally significant vessels because of drastic change of temperature along the blood vessels as shown in Fig. 9(b)–(d) when a lumped power optimization was used, or some cold spots with smaller cold strips (Fig. 5(d)) when using optimization based on local temperature to tune its power at each location. The complexity of existing thermally significant blood vessels plays a very important role in successful hyperthermia treatments. This complexity is related to mass flow rates of vessels, inlet temperatures of vessels, and directions of vessels. In addition, the results also indicate that a heating

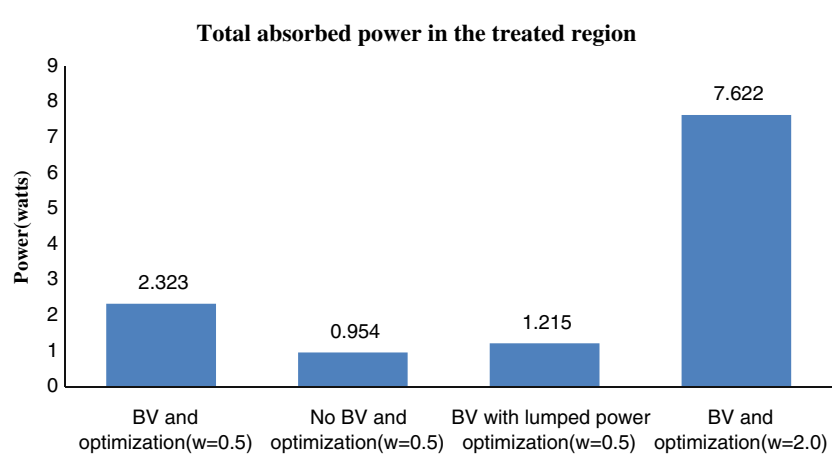

Fig. 10. Total absorbed power at the treated region for optimization with four different conditions. BV means vasculature presents in the treated region; *w* means the blood perfusion rate; optimization means optimization with fine spatial power deposition; and lumped optimization means optimization with lumped power deposition in the desired treated region on minimum cost function (units in figure, *w*: kg m^{-3} s^{-1}).

system with fine spatial power deposition ability is able to tune its power to effectively reduce the convective effect of thermally significant vessels to some local cold spots and/or small cold strips along the blood vessels, while a heating system with coarse spatial power deposition ability is not able to effectively reduce the convective effect and hence leave much larger cold strips along the blood vessels.

Comparing the temperatures and power depositions among blood perfusion rates of 2.0, 0.5 and 0.123 kg m^{-3} s^{-1} with a fine spatial power deposition optimization, their patterns were all similar, except the power level was higher and cold spots/strips were larger for a greater perfusion rate. And they all could result in homogeneous therapeutic temperature distributions in the treated regions. This indicates that a powerful heating system with high resolution of power deposition is important to overcome or effectively limit the cooling effect of blood vessels on the temperature distribution when a temperature imaging system is employed to map the temperature distribution and an optimization algorithm is used to determine the local power required. To further reduce the effect of large blood vessels on the temperature distribution in the desired treated region, preheating the upstream region for thermally significant vessels is a feasible way to raising the blood temperature before it runs into the desired treated region. A powerful heating system with fine spatial resolution and a good image/temperature mapping system are necessary in order to preheat the blood vessels without overheating the surrounding normal tissues.

The amount of total absorbed power in the treated region shown in Fig. 10 indicates that the total power for the case with blood vessels was much higher than that without blood vessels present. The power depositions shown in Figs. 5(f)–(h) and 8(f)–(h) display that the powers deposited in the blood vessels and surrounding areas were the most significantly different. The total power for the blood vessels was even higher than that for perfusion and boundary conduction.

5. Conclusion

To produce a uniform therapeutic temperature distribution in the desired treated region while minimizing the overheating of the surrounding normal tissue is desirable for hyperthermia treatment. To reach this goal requires a powerful heating system that is able to deposit power in the treated region to raise the temperature of the entire treated region up to the desired value and overcome the energy taken away by blood perfusion, boundary conduction, and blood flow from the vasculature. This study employed a 3D tissue model embedded with a countercurrent blood vessel network to simulate the treated tumor region and used optimization to determine the absorbed power deposition for different conditions. The temperature results after optimization show the cold spots and/or cold strips along the blood vessels. These temperatures display the tremendous effects of blood vessels on the resulting heating temperature and the limitation of heating systems. A powerful heating system with fine spatial resolution for power deposition has a better ability to deliver suitable power to locally overcome the convective effect caused by the thermally significant vessels. Although a heating system with fine power deposition is a very important factor during treatment, the complexity of existing thermally significant blood vessels plays a crucial role in successful hyperthermia treatments. This complexity is related to mass flow rates, inlet temperatures, and directions of vessels. Therefore, prior to hyperthermia treatments, thermally significant blood vessels should be identified and handled carefully in order to reduce their cooling effects on the desired treated region, particularly to those vessels flowing into the treated region.

References

[1] H.S. Tharp, R.B. Roemer, Optimal power deposition with finite-sized, planar hyperthermia applicator arrays, IEEE Trans. Biomed. Eng. 39 (6) (1992) 569–579.
[2] W.L. Lin, T.C. Liang, J.Y. Yen, H.L. Liu, Y.Y. Chen, Optimization of power deposition and a heating strategy for external ultrasound thermal therapy, Med. Phys. 28 (10) (2001) 2172–2181.
[3] J.C. Kumaradas, M.D. Sherar, Optimization of a beam shaping bolus for superficial microwave hyperthermia waveguide applicators using a finite element method, Phys. Med. Biol. 48 (1) (2003) 1–18.
[4] T.Y. Cheng, K.C. Ju, C.S. Ho, Y.Y. Chen, H. Chang, W.L. Lin, Split-focused ultrasound transducer with multidirectional heating for breast tumor thermal surgery, Med. Phys. 35 (4) (2008) 1387–1397.
[5] H.H. Pennes, Analysis of tissue and arterial blood temperature in the resting human forearm, J. Appl. Phys. 1 (1948) 93–122.
[6] M.M. Chen, K.R. Holmes, Microvascular contributions in tissue heat transfer, Ann. N.Y. Acad. Sci. 335 (1980) 137–150.
[7] J.J.W. Lagendijk, M. Schellekens, J. Schipper, P.M. van der Linden, A three-dimensional description of heating patterns in vascularised tissues during hyperthermia treatment, Phys. Med. Biol. 29 (1984) 495–507.
[8] S. Weinbaum, L M Jiji, A new simplified bioheat equation for the effect of blood flow on local average tissue temperature, ASME J. Biomech. Eng. 107 (1985) 131–139.
[9] J.J.W. Lagendijk, J. Mooibroek, Hyperthermia treatment planning, Recent Results Cancer Res. 101 (1986) 119–131.
[10] L.M. Jiji, S. Weinbaum, D.E. Lemons, Theory and experiment for the effect of vascular microstructure on surface tissue heat transfer – Part II: Model formulation and solution, ASME J. Biomech. Eng. 106 (1984) 331–341.
[11] J.C. Chato, Heat transfer to blood vessels, ASME J. Biomech. Eng. 110 (1980) 110–118.
[12] H.W. Huang, C.L. Chan, R.B. Roemer, Analytical solutions of Pennes bio-heat transfer equation with a blood vessel, ASME J. Biomech. Eng. 116 (1994) 208–212.
[13] H.W. Huang, Simulation of large vessels in hyperthermia therapy, M.S. Thesis, University of Arizona, Tucson, AZ, 1992.
[14] J.W. Baish, Heat transport by counter current blood vessels in the presence of an arbitrary temperature gradient, ASME J. Biomech. Eng. 112 (1990) 207–211.
[15] J.W. Baish, P.S. Ayyaswamy, K.R. Foster, Small-scale temperature fluctuations in perfused tissue during local hyperthermia, ASME J. Biomech. Eng. 108 (1986) 246–260.
[16] J.W. Baish, P.S. Ayyaswamy, K.R. Foster, Heat transport mechanisms in vascular tissues: a model comparison, ASME J. Biomech. Eng. 108 (1986) 324–330.
[17] J.W. Baish, K.R. Foster, P.S. Ayyaswamy, Perfused phantom models of microwave irradiated tissue, ASME J. Biomech. Eng. 108 (1986) 239–245.
[18] C.K. Charney, R.C. Levin, Heat transfer normal to paired arterioles and venules embedded in perfused tissue during hyperthermia, ASME J. Biomech. Eng. 110 (1988) 277–282.
[19] Z.P. Chen, R.B. Roemer, The effects of large blood vessels on temperature distributions during simulated hyperthermia, ASME J. Biomech. Eng. 114 (1992) 473–481.
[20] J. Crezee, J.J.W. Lagendijk, Experimental verification of bio-heat transfer theories: measurement of temperature profiles around large artificial vessels in perfused tissues, Phys. Med. Biol. 35 (1990) 905–923.
[21] R. Rawnsley, R.B. Roemer, A. Dutton, The simulation of large vessel effects in experimental hyperthermia, ASME J. Biomech. Eng. 116 (1994) 256–262.
[22] G.M.J.V. Leeuwen, A.N.T.J. Kotte, B.W. Raaymakers, J.J.W. Lagendijk, Temperature simulations in tissue with a realistic computer generated vessel network, Phys. Med. Biol. 45 (2000) 1035–1049.
[23] H.S. Kou, T.C. Shih, W.L. Lin, Effect of the directional blood flow on thermal dose distribution during thermal therapy: an application of a Green's function based on the porous model, Phys. Med. Biol. 48 (11) (2003) 1577–1589.
[24] H.W. Huang, Z.P. Chen, R.B. Roemer, A countercurrent vascular network model of heat transfer in tissues, J. Biomech. Eng. 118 (1996) 120–129.
[25] S. Devashish, R.B. Roemer, Readdressing the issue of thermally significant blood vessels using a countercurrent vessel network, ASME J. Biomech. Eng. 128 (2006) 210–216.
[26] J.W. Baish, Formulation of a statistical model of heat transfer in perfused tissue, J. Biomech. Eng. ASME 116 (1994) 521–527.
[27] T.L. Horng, W.L. Lin, C.T. Liauh, T.C. Shih, Effects of pulsatile blood flow in large vessels on thermal dose distribution during thermal therapy, Med. Phys. 34 (4) (2007) 1312–1320.
[28] L. Lapidus, G.F. Pinder, Numerical Solution of Partial Differential Equations in Science and Engineering, Wiley-Interscience Publication, New York, 1982.
[29] Z.P. Chen, A three dimensional treatment planning program for hyperthermia, Ph.D. Dissertation, University of Arizona, Tucson, AZ, 1989.
[30] Z.P. Chen, R.B. Roemer, Improved Cartesian coordinate finite difference simulations of small cylindrical objects, J. Biomech. Eng. ASME 115 (1993) 119–122.